Influence of Electromagnetic Interaction on Neutron Scattering from Nuclei

W. S. HOGAN
Battelle-Columbus Laboratories, Columbus, Ohio
AND
R. G. SEYLER
Ohio State University, Columbus, Ohio 43210

(Received 26 August 1968)

The influence of the interaction between the magnetic moment of a neutron and the Coulomb field of a target nucleus is investigated. A formalism is developed whereby the interaction can be treated exactly in optical-model calculations. Calculations performed at energies of 0.5, 1.0, 7.0, 14.5, and 24 MeV for Al, Mn, Nb, and Bi indicate that this electromagnetic interaction can be adequately treated in the Born approximation. Whereas the influence on the differential cross section is confined to scattering angles less than 2°, the influence on the polarization extends to larger angles corresponding to minima in the cross section.

I. INTRODUCTION

THE effect of the electromagnetic interaction between a neutron and a target nucleus can be important in the interpretation of scattering data. In this study, the influence of the interaction between the magnetic moment of the neutron and the Coulomb field of the target is evaluated. This electromagnetic term is relatively long range (having a $1/r^3$ dependence) and is of spin-orbit form. This latter fact indicates a probable influence on polarization phenomena as well as on the differential-scattering cross section and, in the case of neutron-proton scattering, an influence on many of the measurable double- and triple-scattering parameters.

The influence of the magnetic-moment–Coulomb-field interaction on particle scattering was first brought to general attention by Mott[1] when he pointed out the polarizing effects resulting from electron scattering by nuclei. The importance of this force in neutron-nuclei interactions was first pointed out by Schwinger,[2] who calculated in the Born approximation the influence of this interaction on the elastic scattering cross section and on the neutron polarization. His results indicate a rather pronounced effect for small-angle scattering. This magnetic-moment–Coulomb-field interaction is referred to in the literature variously as Mott-Schwinger scattering, Schwinger scattering, and simply electromagnetic scattering. This work will use the first cited term and abbreviate it as MS scattering. Eriksson[3] has pointed out the importance of this electromagnetic scattering for protons. He calculated the effect on polarization for 130-MeV protons scattered from aluminum, carbon, and iron by a high-energy limiting form of the WKB approximation, and concluded that the effect was noticeable up to scattering angles of 10°. Heckrotte[4] performed a similar calculation for proton-carbon scattering at 300 MeV and obtained results similar to those of Eriksson. Sample[5] has treated the effect in the neutron-scattering problem by handling the electromagnetic interaction as a perturbation and using wave functions obtained from hard-sphere scattering as the zero-order approximation. He gets results entirely consistent with those of the other investigators cited. Monahan and Elwyn[6] found an influence on polarization of neutrons with energies less than 1 MeV that extends to angles as large as 24°. They used an approach based on a generalized Born approximation (which allows for the simultaneous evaluation of nuclear and electromagnetic effects) and found the inclusion of electromagnetic scattering to be necessary in interpreting the experimental polarization data of Elwyn *et al.*[7] Redmond[8] pointed out that Monahan and Elwyn's first-order correction to the Born approximation can be an overcorrection and proposed a more accurate approximation using a technique whereby a phase-shift function is calculated at successive distances from the origin in a step-wise manner.

The fact that MS scattering can significantly influence experimental results has been firmly established in the references cited. In addition, the polarization produced by MS scattering has been experimentally demonstrated by Voss and Wilson[9] in the scattering of 100-MeV neutrons from uranium. In all cases, the methods which have been used to calculate the effects of the MS interaction are approximate ones. In most cases the Born approximation has been used. It would seem, therefore, very desirable to develop more accurate techniques for treatment of the MS force and to evaluate systematically the domains of importance for this interaction.

[1] N. F. Mott, Proc. Roy. Soc. (London) **A124,** 425 (1929).
[2] J. Schwinger, Phys. Rev. **73,** 407 (1948).
[3] T. Eriksson, Nucl. Phys. **2,** 91 (1956).
[4] W. Heckrotte, Phys. Rev. **101,** 1406 (1956).
[5] J. T. Sample, Can. J. Phys. **34,** 36 (1956).
[6] J. E. Monahan and A. J. Elwyn, Phys. Rev. **136,** B1678 (1964).
[7] A. J. Elwyn, R. O. Lane, A. Langsdorf, Jr., and J. E. Monahan, Phys. Rev. **133,** B80 (1964).
[8] R. F. Redmond, Phys. Rev. **140,** B1267 (1965).
[9] R. G. P. Voss and R. Wilson, Phil. Mag. **1,** 175 (1956).

The remainder of this paper is divided into three sections. Section II deals with the theory of neutron scattering by spinless targets. There the formalism for dealing with MS scattering is developed. It is also shown that it is feasible to develop and use MS wave functions in optical model calculations in somewhat the same spirit as Coulomb wave functions are used. In Sec. III, the results of the formalism are applied to models to determine the regions of importance of the MS interaction in a systematic manner. Section IV contains the summary and conclusions. The treatment is nonrelativistic in all cases.

II. GENERAL FORMALISM

Preliminaries. The MS force arises from the interaction of the magnetic moment of one particle with the Coulomb field of the other. In the particular case being considered, the anomalous magnetic moment of the neutron and the Coulomb field of the nucleus are involved. The general form of the MS potential is[6]

$$V_{\mathrm{MS}}(r)=\mathrm{const}(\mathbf{l}\cdot\mathbf{s}/r^3),$$

where $\mathbf{l}$ and $\mathbf{s}$ represent the neutron-orbital and spin-angular momenta, respectively. The constant is

$$Ze^2\hbar^2\mu_n/m^2c^2,$$

where Z is the atomic number of the target nucleus, μ_n the neutron magnetic moment, and m the neutron mass; and c, e, and $\hbar$ have their usual meanings.

It would, of course, be possible to solve the Schrödinger equation numerically with such a potential included. This procedure, however, would result in considerable numerical work primarily because of the long-range nature of this force relative to the nuclear forces. The potential V_{MS} extends to distances comparable to electron orbits and, therefore, requires the range of numerical integration of the radial equation for a given partial wave to be extended by orders of magnitude. In addition, the number of partial waves which is necessary to obtain a satisfactory solution is greatly increased over the pure nuclear-force problem.

It appears that a superior method exists for the evaluation of this interaction. The basis for this method appears in a paper by Calogero,[10] although he credits the equations to the earlier fundamental work of Faxen and Holtsmark.[11] That part of Calogero's paper essential to this work is easily developed.

Consider the equation for the radial wave function in the form

$$\varphi_l''(\rho)+\{1-U(\rho)-[l(l+1)/\rho^2]\}\varphi_l(\rho)=0, \quad (1)$$

where $\rho=(2mE/\hbar^2)r=kr$, and $U(\rho)=(2m/\hbar^2)[V(r)/k^2]$.

A comparison of the equivalent integral equation for φ_l,

$$\varphi_l(\rho)=j_l(\rho)-\int_0^\rho [j_l(\rho)n_l(\rho')-n_l(\rho)j_l(\rho')]\times U(\rho')\varphi_l(\rho')\rho'^2d\rho', \quad (2)$$

where $j_l(\rho)$ and $n_l(\rho)$ are the spherical Bessel and Neuman functions, with a solution of the form

$$\varphi_l(\rho)=C_l(\rho)j_l(\rho)-S_l(\rho)n_l(\rho), \quad (3)$$

leads to the following pair of coupled integral equations for $C_l(\rho)$ and $S_l(\rho)$,

$$C_l(\rho)=1-\int_0^\rho n_l(\rho')U(\rho')\times[C_l(\rho')j_l(\rho')-S_l(\rho')n_l(\rho')]\rho'^2d\rho' \quad (4)$$

and

$$S_l(\rho)=-\int_0^\rho j_l(\rho')U(\rho')\times[C_l(\rho')j_l(\rho')-S_l(\rho')n_l(\rho')]\rho'^2d\rho'. \quad (5)$$

After differentiation, these equations yield two coupled differential equations,

$$C_l'(\rho)=-U(\rho)\rho^2n_l(\rho)[C_l(\rho)j_l(\rho)-S_l(\rho)n_l(\rho)] \quad (6)$$

and

$$S_l'(\rho)=-U(\rho)\rho^2j_l(\rho)[C_l(\rho)j_l(\rho)-S_l(\rho)n_l(\rho)]. \quad (7)$$

In Calogero's paper, little more is done with these equations. Instead, a nonlinear equation for $\tan\delta_l(r)$ is derived and its consequences are pursued in detail.

For the present purpose, Eqs. (6) and (7) appear to be more useful. First, they are linear, and therefore are more easily dealt with in terms of both analytical approximations and numerical integration procedures. Further, $C_l(\rho)$ and $S_l(\rho)$ are better-behaved functions than $\tan\delta_l(\rho)$ since they are bounded and more slowly varying. In addition, radial wave functions are obtained through use of (6) and (7), and the effect of the MS potential can be included in optical-model calculations in a manner very similar to that used to account for the Coulomb interaction.

Use of the MS potential in the expression for $U(\rho)$ in Eq. (1) leads to the following equations for C_{lj} and S_{lj}:

$$C_{lj}'(\rho)=-(\lambda_{lj}/\rho)[C_{lj}(\rho)n_l(\rho)j_l(\rho)-S_{lj}(\rho)n_l^2(\rho)] \quad (8)$$

and

$$S_{lj}'(\rho)=-(\lambda_{lj}/\rho)[C_{lj}(\rho)j_l^2(\rho)-S_{lj}(\rho)n_l(\rho)j_l(\rho)], \quad (9)$$

where

$$\lambda_{lj}=(Ze^2\mid\mu_n\mid k/mc^2)\beta_{lj},$$

$\beta_{lj}=l$ for $j=l+\frac{1}{2}$, or $-(l+1)$ for $j=l-\frac{1}{2}$, and the

[10] F. Calogero, Nuovo Cimento **27**, 261 (1963).
[11] H. Faxen and J. Holtsmark, Z. Physik **45**, 307 (1927).

other factors have been previously defined. The two values of β_{lj} are the eigenvalues of the $\mathbf{l}\cdot\mathbf{s}$ operator.

It is convenient to introduce the functions $f_{lj}(\rho)$ and $g_{lj}(\rho)$ defined by

$$S_{lj}(\rho)=t_{lj}f_{lj}(\rho)\exp[-\lambda_{lj}b_l(\rho)] \tag{10}$$

and

$$C_{lj}=g_{lj}(\rho)\exp[\lambda_{lj}b_l(\rho)], \tag{11}$$

where

$$t_{lj}=\tan\delta_{lj}=\lim_{\rho\to\infty}\frac{S_{lj}(\rho)}{C_{lj}(\rho)},$$

$$b_l(\rho)=\int_\rho^\infty\frac{j_l(\rho')n_l(\rho')}{\rho'}d\rho', \tag{12}$$

and

$$\lim_{\rho\to\infty}f_{lj}(\rho)=1;\qquad\lim_{\rho\to\infty}g_{lj}(\rho)=1.$$

The above limits are chosen for convenience, the only necessary condition being that the limit of the ratio f/g be unity. Substitution of these forms into Eqs. (8) and (9) gives

$$f_{lj}'(\rho)=-(\lambda_{lj}/t_{lj})[j_l^2(\rho)/\rho]g_{lj}(\rho)\exp 2\lambda_{lj}b_l(\rho), \tag{13}$$

$$g_{lj}'(\rho)=\lambda_{lj}t_{lj}[n_l^2(\rho)/\rho]f_{lj}(\rho)\exp[-2\lambda_{lj}b_l(\rho)]. \tag{14}$$

Through integration of Eqs. (13) and (14) it is possible to express $f_{lj}(\rho)$ and $g_{lj}(\rho)$ as solutions to the nonlinear Volterra equation of the second kind. From these integral equations, it can be shown that one can express $f_{lj}(\rho)$ and $g_{lj}(\rho)$ as

$$f_{lj}(\rho)=1/t_{lj}F_{lj}^{(1)}(\rho)+F_{lj}^{(2)}(\rho), \tag{15}$$

$$g_{lj}(\rho)=t_{lj}(\rho)G_{lj}^{(1)}(\rho)+G_{lj}^{(2)}(\rho), \tag{16}$$

where $F_{lj}^{(1)}(\rho)$, $F_{lj}^{(2)}(\rho)$, $G_{lj}^{(1)}(\rho)$, and $G_{lj}^{(2)}(\rho)$ are independent of t_{lj}.

By using Eqs. (15) and (16) in Eqs. (13) and (14) and equating coefficients of like powers of t_{lj}, the following set of equations results:

$$F_{lj}^{(1)\prime}(\rho)=-\lambda_{lj}[j_l^2(\rho)/\rho]G_{lj}^{(2)}(\rho)\exp 2\lambda_{lj}b_l(\rho), \tag{17}$$

$$G_{lj}^{(2)\prime}(\rho)=\lambda_{lj}[n_l^2(\rho)/\rho]F_{lj}^{(1)}(\rho)\exp[-2\lambda_{lj}b_l(\rho)], \tag{18}$$

$$F_{lj}^{(2)\prime}(\rho)=-\lambda_{lj}[j_l^2(\rho)/\rho]G_{lj}^{(1)}(\rho)\exp 2\lambda_{lj}b_l(\rho), \tag{19}$$

$$G_{lj}^{(1)\prime}(\rho)=\lambda_{lj}[n_l^2(\rho)/\rho]F_{lj}^{(2)}(\rho)\exp[-2\lambda_{lj}b_l(\rho)]. \tag{20}$$

The appropriate asymptotic values are given through Eqs. (15) and (16), and the expression immediately following Eq. (12). They are

$$F_{lj}^{(1)}\sim 0,\qquad G_{lj}^{(1)}\sim 0,$$
$$F_{lj}^{(2)}\sim 1,\qquad G_{lj}^{(2)}\sim 1. \tag{21}$$

From Eqs. (10) and (11) and Eqs. (15) and (16), the tangent of the phase shift t_{lj} can be written

$$t_{lj}=\frac{F_{lj}^{(1)}(\rho_c)\exp-2\lambda_{lj}b_l(\rho_c)-\tan\delta_{lj}(\rho_c)G_{lj}^{(2)}(\rho_c)}{\tan\delta_{lj}(\rho_c)G_{lj}^{(1)}(\rho_c)-F_{lj}^{(2)}(\rho_c)\exp-2\lambda_{lj}b_l(\rho_c)}, \tag{22}$$

where $\tan\delta_{lj}(\rho_c)$ is the phase-shift function

$$\tan\delta_{lj}(\rho)[=S_{lj}(\rho)/C_{lj}(\rho)]$$

evaluated at a radius r_c beyond which the nuclear potential is negligible. The quantity $\delta_{lj}(\rho_c)$ is the phase shift that would result from the $r\leq r_c$ part of the total potential. The actual phase shift $\delta_{lj}(\infty)$ will differ from $\delta_{lj}(\rho_c)$ only because of the MS potential acting in the region $r>r_c$.

Next, approximate analytical solutions to Eqs. (17)–(21) are developed and the resulting formula for Eq. (22) is compared with some approximations in the literature. A discussion of the exact numerical solutions of the above equations is postponed until later.

Approximate Solutions. In order to establish the basis for the approximate solutions, it is necessary to consider the behavior of certain integrals which are involved. Explicit forms for these integrals are given by Redmond[8] and are given here for convenience. To facilitate later reference, the symbols $a_l(\rho)$, and $c_l(\rho)$ are introduced:

$$a_l(\rho)=\int_\rho^\infty\frac{j_l^2(\rho')}{\rho'}d\rho'$$
$$=[2l(l+1)]^{-1}\{1-\rho^2[(1-l\rho^{-2})j_l^2(\rho)+j_{l-1}^2(\rho)-2l\rho^{-1}j_l(\rho)j_{l-1}(\rho)]\}, \tag{23}$$

$$b_l(\rho)=\int_\rho^\infty\frac{j_l(\rho')n_l(\rho')}{\rho'}d\rho'$$
$$=\frac{-\rho^2}{2l(l+1)}\{(1-l\rho^{-2})j_l(\rho)n_l(\rho)+j_{l-1}(\rho)n_{l-1}(\rho)-[j_l(\rho)n_{l-1}(\rho)+j_{l-1}(\rho)n_l(\rho)]l\rho^{-1}\}, \tag{24}$$

$$c_l(\rho)=\int_\rho^\infty\frac{n_l^2(\rho')}{\rho'}d\rho'$$
$$=[2l(l+1)]^{-1}\{1-\rho^2[(1-l\rho^{-2})n_l^2(\rho)+n_{l-1}^2(\rho)-2l\rho^{-1}n_l(\rho)n_{l-1}(\rho)]\}. \tag{25}$$

The $\rho \ll l$ limiting forms for the functions $j_l(\rho)$ and $n_l(\rho)$,

$$\lim_{\rho\to 0} j_l(\rho) \to \frac{\rho^l}{1\cdot 3\cdot 5\cdot 7\cdot \cdots \cdot (2l+1)} \tag{26}$$

and

$$\lim_{\rho\to 0} n_l(\rho) \to -\frac{1\cdot 3\cdot 5\cdot 7\cdot \cdots \cdot (2l-1)}{\rho^{l+1}}, \tag{27}$$

may be used to obtain the behavior of the three functions for small ρ values,

$$\lim_{\rho\to 0} a_l \to 1/2l(l+1), \tag{28}$$

$$\lim_{\rho\to 0} b_l(\rho) \to -1/(2l+1)\rho, \tag{29}$$

$$\lim_{\rho\to 0} c_l(\rho) \to [(2l-1)!!]^2/2(l+1)\rho^{2l+2}. \tag{30}$$

The function $a_l(\rho)$ is seen to be constant (for fixed l) at small ρ, whereas $c_l(\rho)$ changes rapidly and is singular at the origin.

For the exponential factors in Eqs. (17)–(20) to be replaced by unity, it is necessary that $2\lambda_{lj} b_l(\rho) \ll 1$. Substituting in this inequality the definition of λ_{lj} following Eq. (9) and the small ρ approximation to $b_l(\rho)$ leads to the condition $r \gg 3\times 10^{-14}$ cm, where r is the radial distance from the center of the nucleus. As this quantity (0.3 F) is smaller than a nucleon radius, one can conclude that for $\rho < l$, the exponential factor can be replaced by unity.

Now if one assumes in Eq. (17) that $G_{lj}^{(2)}$ is well represented by its asymptotic value of unity (numerical results verify this assumption for ρ not too small), then

$$F_{lj}^{(1)}(\rho) \approx \lambda_{lj} a_l(\rho). \tag{31}$$

Also, using this result in Eq. (18) and noting [Eq. (23)] that $a_l(\rho) \approx a_l(0)$ over most of the range where $a_l(\rho)$ is appreciably different from zero, one gets

$$G_{lj}^{(2)}(\rho) \approx 1 - \lambda_{lj}^2 a_l(0) c_l(\rho). \tag{32}$$

In applying the same kind of approximations to Eqs. (19) and (20) one finds

$$F_{lj}^{(2)}(\rho) \approx 1 \tag{33}$$

and

$$G_{lj}^{(1)}(\rho) \approx -\lambda_{lj} c_l(\rho). \tag{34}$$

The range of validity of these approximations can be determined by examining the result of substituting Eqs. (31)–(34) into the differential equations (17)–(20).

In order for Eqs. (31) and (32) to be good approximations, it can be seen that $|\lambda_{lj}^2 a_l(0) c_l(\rho)| \ll 1$ should be true. More explicitly, using Eqs. (29) and (30) in this inequality, one gets for a necessary condition

$$\rho^{2l+2} \gg \lambda_{lj}^2 [(2l-1)!!]^2/4l(l+1)^2. \tag{35}$$

For Eqs. (33) and (34) to be valid, it is necessary that $F_{lj}^{(2)\prime}$ be small, or $|\lambda_{lj}^2 (j_l^2(\rho)/\rho) c_l(\rho)| \ll 1$, which can be expressed through the use of Eq. (30) as

$$\rho^3 \gg \lambda_{lj}^2/(2l+1)^2 2(l+1). \tag{36}$$

It is interesting to use these approximate results in Eq. (22), and to compare the resulting form with other approximations. The result of Eqs. (31)–(34) substituted in Eq. (22) gives, after a little rearranging,

$$t_{lj} = \frac{\tan\delta_{lj}(\rho_c) - \lambda_{lj} a_l(\rho_c) \exp[-2\lambda_{lj} b_l(\rho_c)] - \lambda_{lj}^2 \tan\delta_{lj}(\rho_c) a_l(0) c_l(\rho_c)}{\exp[-2\lambda_{lj} b_l(\rho_c)] + \tan\delta_{lj}(\rho_c) \lambda_{lj} c_l(\rho_c)}. \tag{37}$$

For comparison, the plane-wave Born approximation gives

$$t_{lj} = \tan\delta_{lj}(\rho_c) - \lambda_{lj} a_l(\rho_c), \tag{38}$$

and Monahan and Elwyn[7] derive

$$t_{lj} = \frac{[1+\lambda_{lj} b_l(\rho_c)] \tan\delta_{lj}(\rho_c) - \lambda_{lj} a_l(\rho_c)}{1 - \lambda_{lj} b_l(\rho_c) + \lambda_{lj} c_l(\rho_c) \tan\delta_{lj}(\rho_c)}. \tag{39}$$

The Monahan and Elwyn result is very much like Eq. (37) and, in fact, they are identical through terms of the order of λ_{lj} if $\lambda_{lj} b_l(\rho) \ll 1$. It has already been established that this is a good approximation.

The same approximations give, for the radial wave function outside the nuclear radius,

$$\phi_l(\rho) \approx \left\{1 - \lambda_{lj}^2 a_l(0) c_l(\rho) - \lambda_{lj} c_l(\rho) \left[\frac{\tan\delta_{lj}(\rho_c) - \lambda_{lj} a_l(\rho_c) - \lambda_{lj}^2 a_l(0) c_l(\rho_c) \tan\delta_{lj}(\rho_c)}{1 + \lambda_{lj} \tan\delta_{lj}(\rho_c) c_l(\rho_c)}\right]\right\} j_l(\rho)$$
$$- \left\{\lambda_{lj} a_l(\rho) + \left[\frac{\tan\delta_{lj}(\rho_c) - \lambda_{lj} a_l(\rho_c) - \lambda_{lj}^2 a_l(0) c_l(\rho_c) \tan\delta_{lj}(\rho_c)}{1 + \lambda_{lj} \tan\delta_{lj}(\rho_c) c_l(\rho_c)}\right]\right\} n_l(\rho). \tag{40}$$

Exact Solutions. Equations (17)–(20) with the boundary conditions, Eq. (21), can, of course, be solved exactly numerically. Inspection shows the two pairs of coupled equations to be identical. That is, Eqs. (17) and (18) are identical to Eqs. (19) and (20), so the same program will solve each set and it is only necessary to apply the appropriate boundary conditions. For convenience in applying the boundary conditions, a change of variable was made as $z = 1/\rho$. Thus, the asymptotic values of the functions were applied at

$z=0$ and the numerical integrations performed outward to a desired value of z on the CDC-6400 digital computer. The method used was the well-known Runge-Kutta method as applied to simultaneous equations.[12] The inherent error in this method is of the order of $(\Delta z)^5$, or for the cases done here, 10^{-10} or less since the largest value of Δz ever used was 10^{-2}.

It is perhaps appropriate to point out here that this procedure requires much less numerical work than would direct integration of the Schrödinger equation. Further, it provides a better physical basis for interpreting various approximate methods.

It is clear that the general technique described here could be applied to the scattering of protons by nuclei. To make this application it is only necessary to replace the spherical Bessel functions by the appropriate Coulomb wave functions. The approximate solutions are not as useful in this case since the analogs to Eqs. (23)–(25) are not known. It is perhaps also true that the effects are not as interesting in the proton case due to the large small-angle Coulomb scattering cross section, which would tend to obscure the MS influence on polarization and differential cross section, both of which are most influenced at small scattering angles.

Optical Model. One of the objectives of this study was to assess the effects of the MS force on neutron scattering. The most straightforward way to do this seemed to be to compare the results of optical model calculations with and without the MS term in the potential. To this end, the optical model program CLOUDY, written and used by Cassola and Koshel[13] in optical-model studies, was obtained and modified to include the MS term when desired. The form of the nuclear potential used for this problem was

$$V(r)=-V_c f(r)-iW_c g(r)+V_{so}r^{-1}(df/dr)\,\boldsymbol{\sigma}\cdot\mathbf{l}(\hbar/m_\pi c)^2, \tag{41}$$

where $f(r)$ is the Woods-Saxon form

$$f(r)=\{1+\exp[(r-R)/a_s]\}^{-1} \tag{42}$$

and $g(r)$ is a surface absorption term of the form

$$g(r)=4\exp[(r-R)/a_D]\{1+\exp[(r-R)/a_D]\}^{-2}. \tag{43}$$

The usual r^{-3} radial dependence of the MS potential was employed for $r>R$ (the nuclear radius), and for $r<R$ the value of the MS potential at the nuclear radius was assumed which is consistent with the assumption of a uniform charge density for the nucleus. This constant MS potential for $r<R$ is completely negligible in comparison with the nuclear potential, Eq. (41), in this same region. Thus only in the region of r between R and r_c must one include simultaneously both the nuclear and MS potentials. No attempt was made to find optimum optical-model parameters based on experimental data, but rather, the parameters chosen were based on the Elwyn *et al.*[7] evaluations of the nonlocal parameters of Perey and Buck.[14] The basic parameters used in the calculations were

$$V_c=47.20-0.27E \text{ MeV},$$
$$W_c=9.6 \text{ MeV},$$
$$V_{so}=7.2 \text{ MeV},$$
$$a_D=0.66 \text{ fm},$$
$$a_s=0.47 \text{ fm},$$

and

$$R=1.27A^{1/3} \text{ fm}.$$

For neutron energies less than about 5 MeV, the effects of compound-elastic scattering must be included. In the optical model, this contribution is included in the reaction cross section. Compound elastically scattered neutrons are unpolarized and have a different angular distribution than those scattered via the shape-elastic process, and hence exert an influence on the experimentally determined polarizations and cross sections. To account for this effect in the present calculations, a simple model used by Perey and Buck[14] was adopted. In this model, the total compound-elastic cross section σ_{CE} was taken to be the optical-model-reaction cross section σ_r less the experimentally determined nonelastic cross section σ_N. The process was assumed to be isotropic, and the polarization is then diluted by the ratio

$$\frac{d\sigma_s(\theta)}{d\Omega}\Big/\left(\frac{d\sigma_s(\theta)}{d\Omega}+\frac{\sigma_{CE}}{4\pi}\right),$$

where $d\sigma_s(\theta)/d\Omega$ is the shape-elastic differential cross section.

The optical-model calculations determine the phase shifts $\delta_{lj}(\rho_c)$ to be used in Eq. (22). That is, by using the optical-model program to solve the Schrödinger equation numerically out to ρ_c with the complex potential as described and including the MS potential, the phase shifts $\delta_{lj}(\rho_c)$ can be found. This, of course, is the phase shift that would result if the potential included in its determination were the entire potential, or, in other words, if the MS potential could be neglected for $\rho>\rho_c$. The tangent of the actual phase shift, then, as given by Eq. (22), is the large r limit of the phase-shift function. The cutoff value ρ_c must only be large enough to include all effect of the nuclear potential.

Since the interaction is assumed to be independent of the spin of the target nucleus, it is permissible to treat the scattering as that from a target of zero spin. The treatment of scattering of spin-$\frac{1}{2}$ particles by spin-zero targets is well known and the results are readily avail-

[12] J. B. Scarborough, *Numerical Mathematical Analysis* (The Johns Hopkins Press, Baltimore, 1950), 2nd ed., p. 302.

[13] R. L. Cassola and R. D. Koshel, Nuovo Cimento **47**, 303 (1967).

[14] F. P. Perey and B. Buck, Nucl. Phys. **32**, 353 (1962).

able in the literature.[15–17] If the scattering is analyzed in terms of partial waves, the pertinent results for scattering of an unpolarized beam can be expressed as

$$\sigma_s=\frac{\pi}{k^2}\sum_{l=0}^{\infty}\{(l+1)\mid 1-\eta_{lj}^{+}\mid^2+l\mid 1-\eta_{lj}^{-}\mid^2\},\tag{44}$$

$$\sigma_r=\frac{\pi}{k^2}\sum_{l=0}^{\infty}\{(l+1)(1-\mid\eta_{lj}^{+}\mid^2)+l(1-\mid\eta_{lj}^{-}\mid^2)\},\tag{45}$$

$$d\sigma_s(\theta)/d\Omega=\mid g(\theta)\mid^2+\mid h(\theta)\mid^2,\tag{46}$$

$$\mathbf{P}_{\mathrm{S.E.}}(\theta)=\frac{2\,\mathrm{Re}g^*(\theta)h(\theta)}{d\sigma_s(\theta)/d\Omega}\,\mathbf{n},\qquad(\mathbf{n}=\mathbf{k}_i\times\mathbf{k}_f)\tag{47}$$

where

$$g(\theta)=(2ik)^{-1}\sum_{l=0}^{\infty}[(l+1)(\eta_l^{+}-1)+l(\eta_l^{-}-1)]P_l(\cos\theta),\tag{48}$$

$$h(\theta)=(2k)^{-1}\sum_{l=1}^{\infty}(\eta_l^{+}-\eta_l^{-})P_l^{1}(\cos\theta),\tag{49}$$

$$\eta_l^{+}=\eta_{l,l+1/2}=\exp(2i\delta_{l,l+1/2}),$$

and

$$\eta_l^{-}=\eta_{l,l-1/2}=\exp(2i\delta_{l,l-1/2}).$$

The observable quantities defined on the left-hand side of the above equations are σ_s—total-scattering cross section, σ_r—reaction cross section, $d\sigma_s(\theta)/d\Omega$—differential-scattering cross section, and $P(\theta)$ is the neutron polarization after scattering. Further, Re denotes the real part of the quantity involved, and $P_l(\cos\theta)$ and $P_l^1(\cos\theta)$ represent Legendre polynomials and associated Legendre polynomials, respectively.

The series in Eq. (49) converges slowly when MS scattering is included. However, the Born approximation gives accurate results for sufficiently large l and hence can be used to include the effect of all l above some appropriate cutoff value l_c. This type of correction was carried out by Sample.[5] The resulting equation for $h(\theta)$ is

$$h(\theta)=(2k)^{-1}\sum_{l=1}^{\infty}\left\{(\eta_l^{+}-\eta_l^{-})+\left(\frac{2l+1}{l(l+1)}\right)i\gamma k\right\}\times P_l^{1}(\cos\theta)-\tfrac{1}{2}(i\gamma)\cot\tfrac{1}{2}\theta.\tag{50}$$

In this expression, γ is a constant related to the MS interaction,

$$\gamma=\mid\mu_n\mid Z(e^2/mc^2).\tag{51}$$

In all other sums, the convergence is rapid, and one may achieve sufficient accuracy by truncating the series with a reasonable value of l_c.

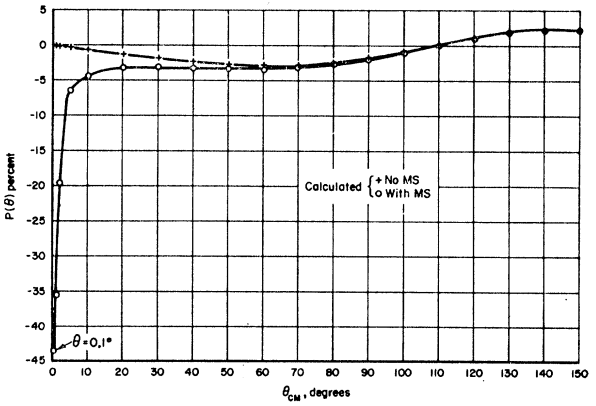

FIG. 1. Polarization of 0.5-MeV neutrons scattered by Al.

In addition to the numerical treatments with and without MS scattering, it is also of interest for comparison purposes to include the results of the Born approximation. In the Born approximation

$$t_{lj}=\tan\delta_{lj}(\rho_c)-\lambda_{lj}a_l(\rho_c),\tag{38}$$

and the MS contribution to the scattering amplitude $h_{\mathrm{MS}}(\theta)$ is[18]

$$h_{\mathrm{MS}}(\theta)=-\tfrac{1}{2}(i\gamma)\cot\tfrac{1}{2}\theta.\tag{52}$$

In the application here, t_{lj} was found from Eq. (38) and the calculations were carried out as in the exact case.

The ρ_c and l_c values suggested by Hodgson[19] for the optical model are $l_c=2.4\rho_N$ and $\rho_c=\rho_N+7a_s$, where $\rho_N=kR$ and R is the nuclear radius. In addition, it was determined that ~100 mesh points within the nuclear radius gave good results (i.e., changing from 100 to 200 mesh points made only negligible changes in the results). Actually, in most cases l_c, ρ_c, and the number of mesh points were chosen substantially greater than the values given above. It was also found that moderate variation of the charge radius about the nuclear radius had no appreciable influence on the results, so the charge radius was taken to be the nuclear radius in all cases.

III. RESULTS OF THE CALCULATIONS

Typical results of the optical model calculations are presented in Figs. 1–16. Calculations were done for Al, Mn, Nb, and Bi at energies of 0.5, 1, 7, 14.5, and 24 MeV. Those results which are repetitious, or which do not show any features of particular interest, have been omitted. The differential cross sections are compared with experimental data from BNL-400[20] in some cases, and with the optical model results of Agee and

[15] M. L. Goldberger and K. M. Watson, *Collision Theory* (John Wiley & Sons, Inc., New York, 1964), Chap. 7.
[16] T. Y. Wu and T. Ohmura, *Quantum Theory of Scattering* (Prentice-Hall, Inc., Englewood Cliffs, N.J., 1962), Chap. 2.
[17] N. F. Mott and H. S. W. Massey, *The Theory of Atomic Collisions* (Clarendon Press, Oxford, England, 1965), 3rd ed., Chap. 10.
[18] L. Wolfenstein, Ann. Rev. Nucl. Sci. **6**, 43 (1956).
[19] P. E. Hodgson, *The Optical Model of Elastic Scattering* (Clarendon Press, Oxford, England, 1963), Chap. 5.
[20] M. D. Goldberg, V. M. May, and J. R. Stehn, *Angular Distributions in Neutron-Induced Reactions* [Brookhaven National Laboratory (BNL-400), 1962], 2nd ed.

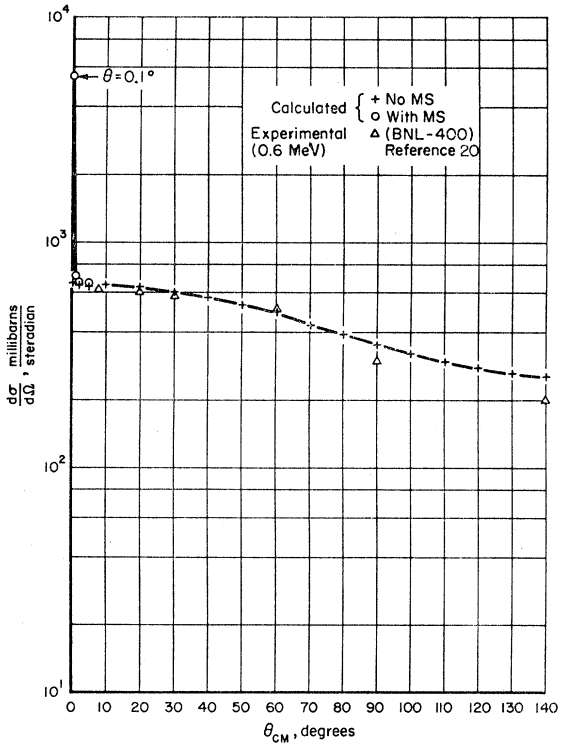

FIG. 2. Differential-scattering cross section for 0.5-MeV neutrons scattered by Al.

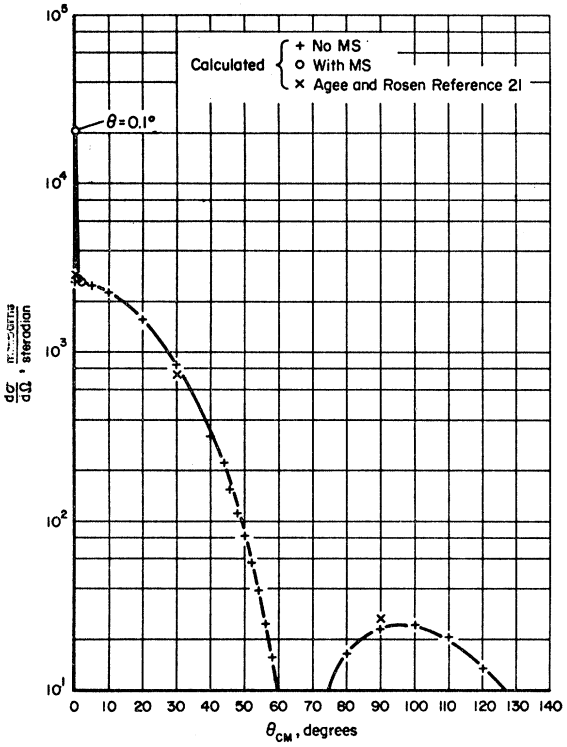

FIG. 4. Differential-scattering cross section for 7-MeV neutrons scattered by Mn.

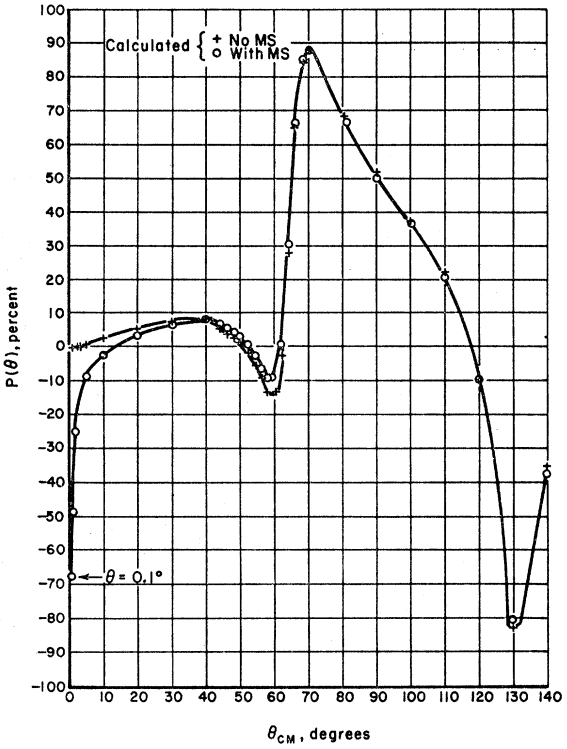

FIG. 3. Polarization of 7-MeV neutrons scattered by Mn.

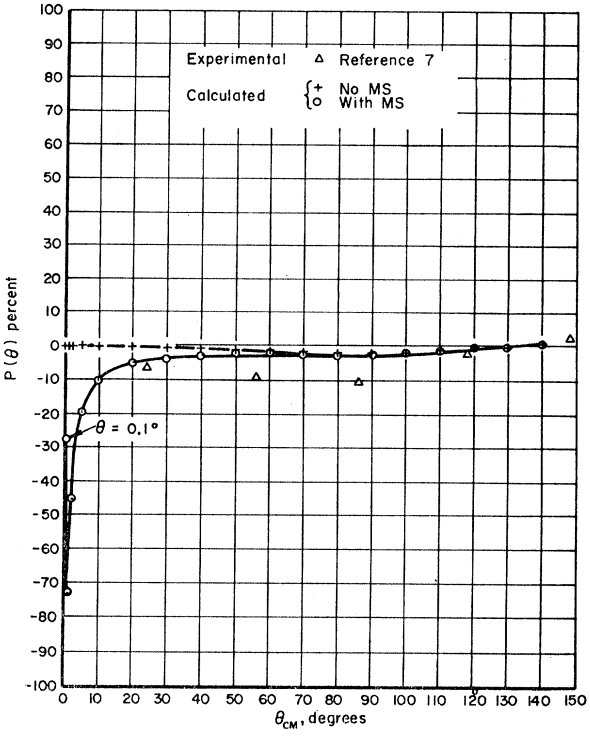

FIG. 5. Polarization of 0.5-MeV neutrons scattered by Nb.

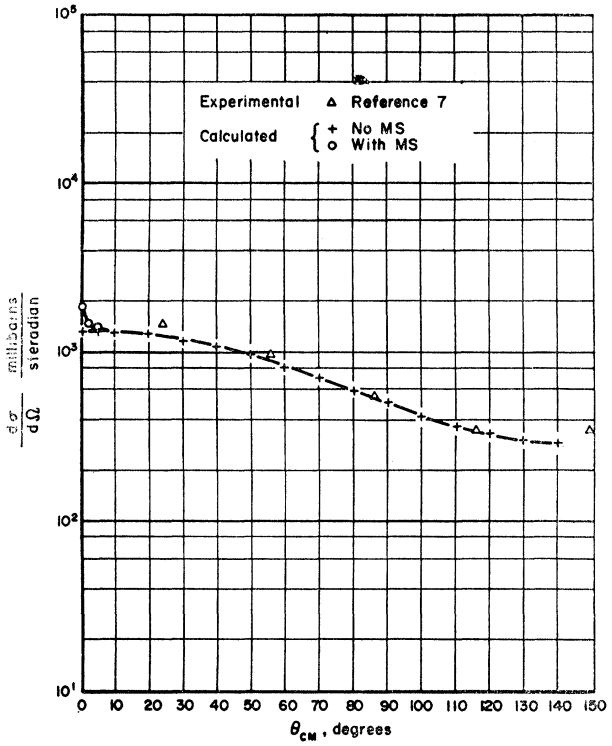

FIG. 6. Differential-scattering cross section for 0.5-MeV neutrons scattered by Nb.

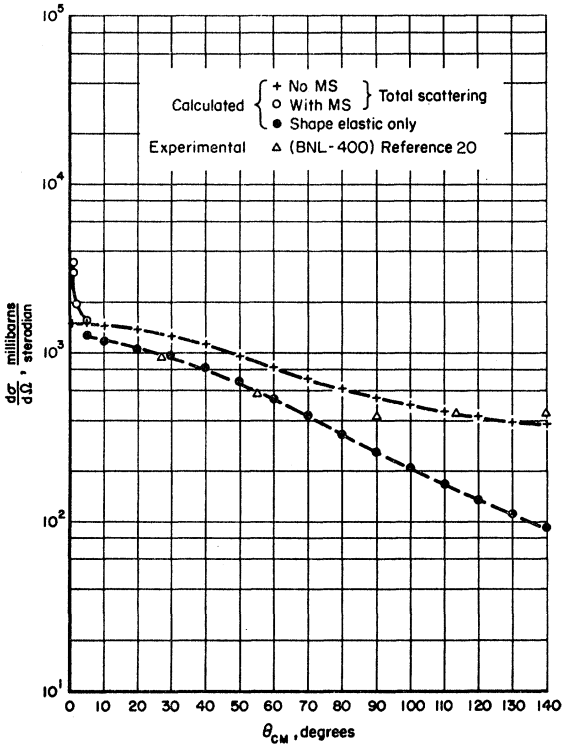

FIG. 8. Differential-scattering cross section for 0.5-MeV neutrons scattered by Bi.

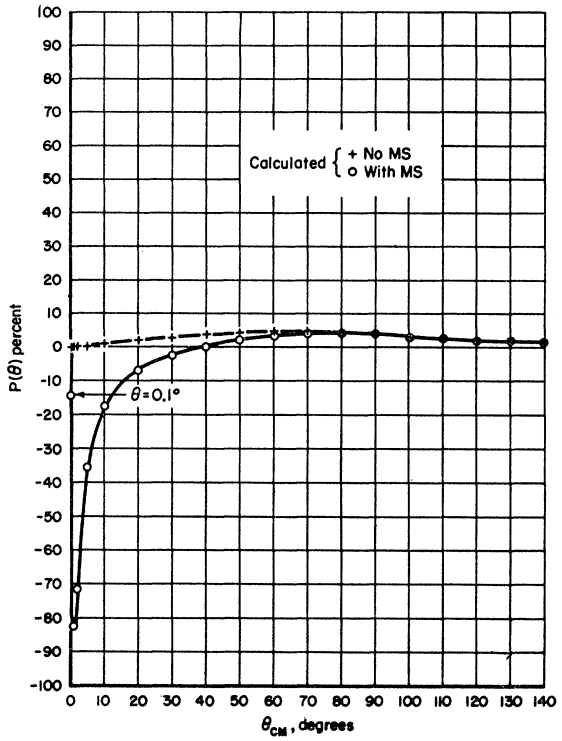

FIG. 7. Polarization of 0.5-MeV neutrons scattered by Bi.

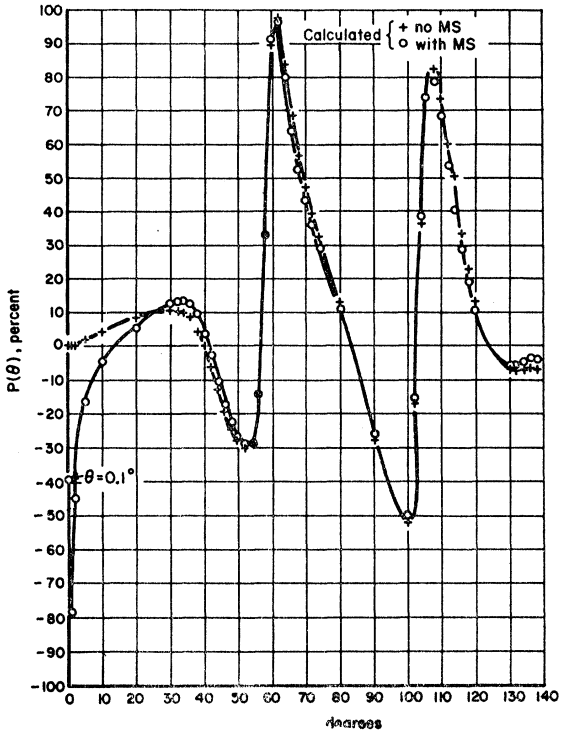

FIG. 9. Polarization of 7-MeV neutrons scattered by Bi.

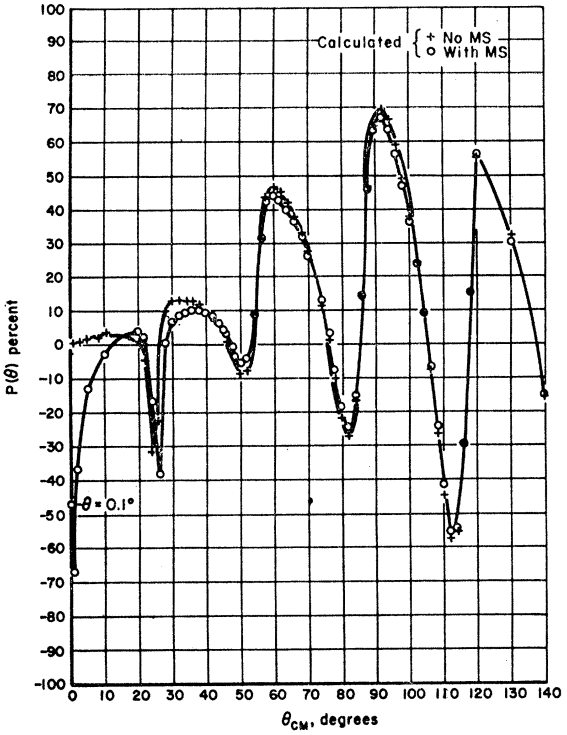

FIG. 10. Polarization of 14.5-MeV neutrons scattered by Bi.

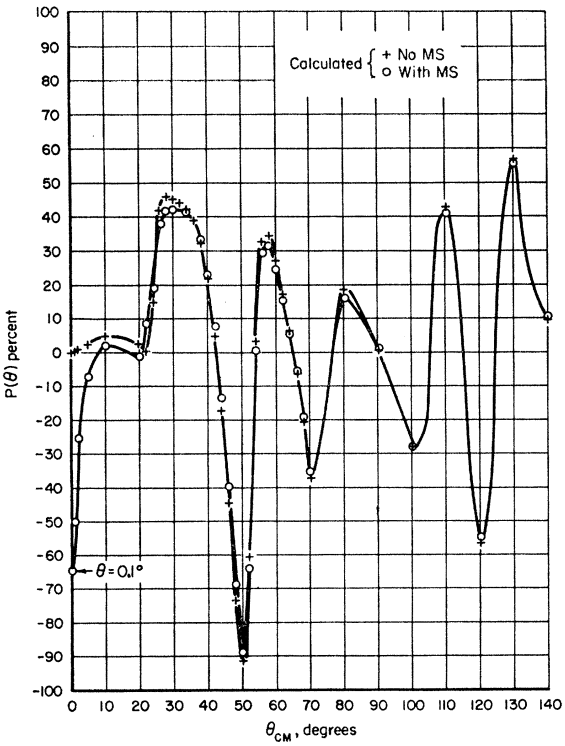

FIG. 12. Polarization of 24-MeV neutrons scattered by Bi.

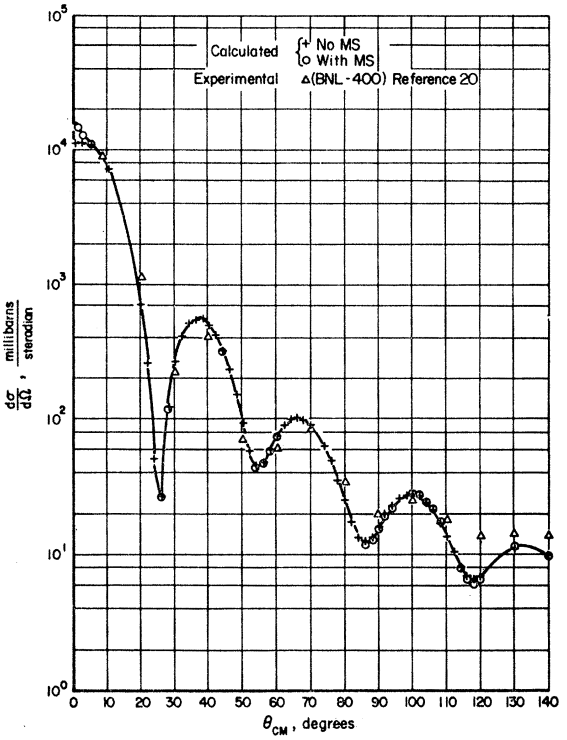

FIG. 11. Differential-scattering cross section for 14.5-MeV neutrons scattered by Bi.

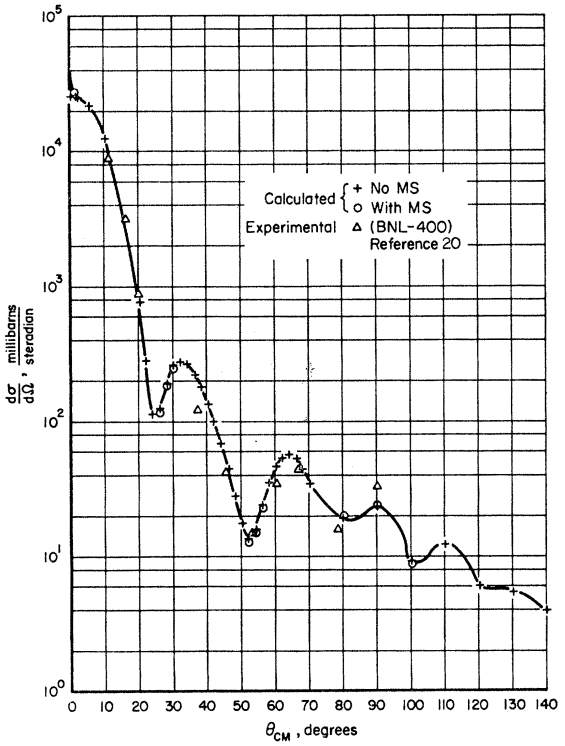

FIG. 13. Differential-scattering cross section for 24-MeV neutrons scattered by Bi.

Rosen[21] in other cases, as noted on the curves. In general, the agreement is good, the only exception being Al at 1 MeV (not shown), and Bi at 0.5 (Fig. 8) and 1 MeV (not shown). These cases of relatively poor agreement are probably attributable to the approximate method of treating compound elastic scattering in the present calculations. The generally good agreement with experiment serves to establish a degree of confidence in the choice of optical model parameters. In general, the inclusion of the MS term has very little influence on $d\sigma(\theta)/d\Omega$ except at very small angles,

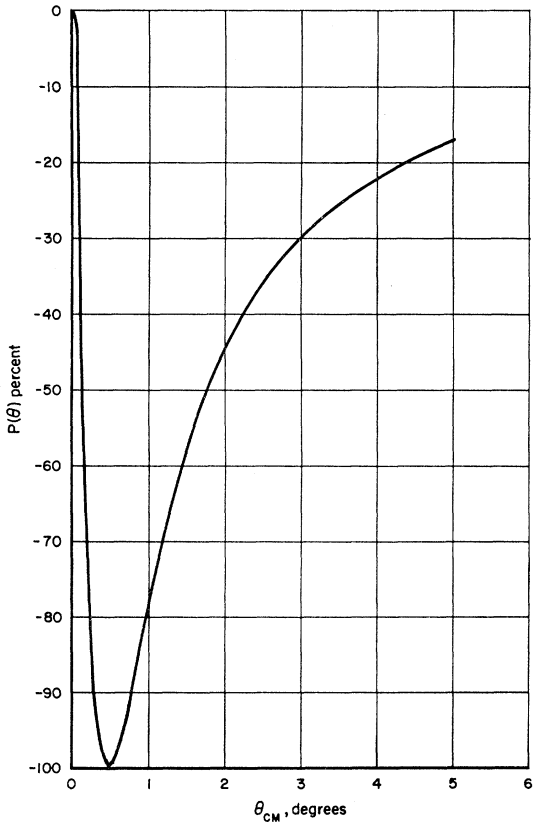

FIG. 14. Small-angle polarization of 7-MeV neutrons scattered by Bi (with MS).

$\sim 2°$ or less. This effect was expected, and is greatest at low energies and for high Z targets, and was given in all cases considered, to an accuracy of about 1% or better by the Born approximation for the phase shifts. In fact, a somewhat unexpected result of the study is that use of the Born approximation for the phase shifts [Eq. (38)] is adequate in all cases for both $d\sigma(\theta)/d\Omega$ and $P(\theta)$. Polarizations calculated with the MS effect included exactly and through use of the Born approximation [Eq. (38)] agree to within 0.5% in all cases. This result can be explained qualitatively

[21] F. P. Agee and L. Rosen, Los Alamos Scientific Laboratory Report No. LA-3538, 1966 (unpublished).

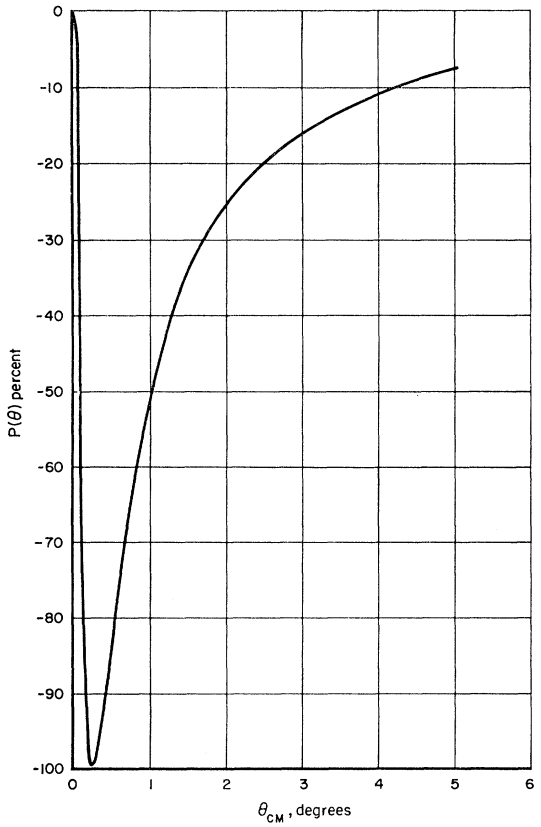

FIG. 15. Small-angle polarization of 24-MeV neutrons scattered by Bi (with MS).

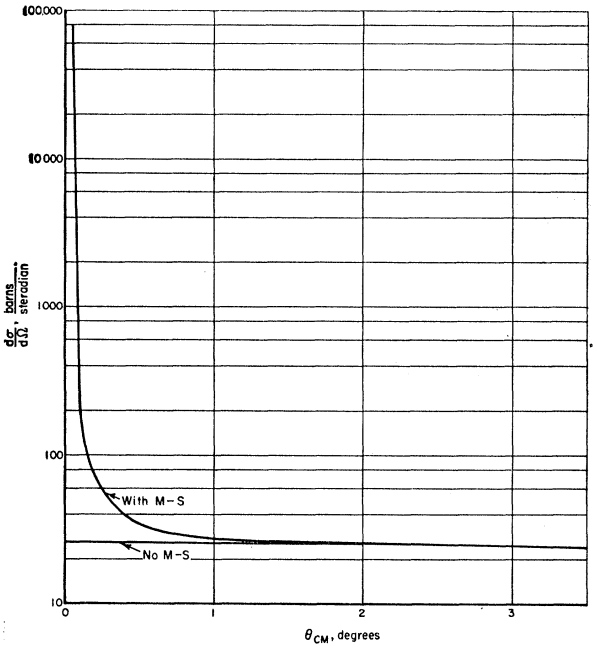

FIG. 16. Small-angle scattering cross section for 24-MeV neutrons scattered by Bi.

on the basis that one expects the Born approximation to be valid when $E \gg V$, and for the values of ρ_c which were used, this condition was always satisfied. Further insight into the validity of the Born approximation is given from the approximate solutions for the phase shifts as given in Eq. (37). The Born approximation is seen to result from Eq. (37) if $c_l(\rho_c)$ is small, and this is the case for ρ_c large. That is, for ρ_c large enough Eqs. (31)–(34) become

$$F_{lj}^{(1)}(\rho) \approx \lambda_{lj} a_l(\rho), \tag{53}$$

$$G_{lj}^{(2)}(\rho) \approx 1, \tag{54}$$

$$F_{lj}^{(2)}(\rho) \approx 1, \tag{55}$$

and

$$G_{lj}^{(1)}(\rho) \approx 0, \tag{56}$$

and these results substituted in Eq. (22) give the Born approximation.

The calculations for $P(\theta)$ gave results that were not entirely expected. The small-angle influence of the MS term previously discussed is clearly present in all cases. This effect, like the small-angle effect on $d\sigma(\theta)/d\Omega$, is generally greatest at low energies and high Z. The calculation for Nb at 0.5 MeV (Fig. 5) substantiates the influence of the MS force as calculated in Refs. 6 and 7, although there is a general lack of agreement with the experimental results of Ref. 7 at 56° and 86°. This "small-angle" effect is seen to exert a significant influence on $P(\theta)$ for Bi at 0.5 MeV at angles as large as 40°–50° (Fig. 7). In all cases, at the low energies investigated, this influence is evident out to 20°, and as just noted, to 50° in the extreme case; however, for the highest energy (24 MeV) this influence is restricted to the 10°–15° range. For all isotopes studied, this small-angle effect is the only one observed at low energies. However, for the higher Z nuclei and at the higher energies, the polarization is seen to be influenced by the MS term in a somewhat different manner. See, for example, Mn at 7 MeV in the 50°–60° range (Fig. 3), and Bi at the higher energies in the 25°–40° range (Figs. 9, 10, and 12). Indeed, Bi at 7 MeV shows an effect at 130°–140° (Fig 9). An examination of the curves indicates that these effects on polarization occur at angles which correspond to regions near minima in the cross-section curve.

The general results of the polarization can be explained qualitatively. At very small angles, the $\cot\frac{1}{2}\theta$ term [see Eq. (50)] dominates the quantity $h(\theta)$ when the MS term is included in the potential. As θ increases, $|h(\theta)|$ tends to become small relative to $|g(\theta)|$ and effects on polarization are not seen, unless $|g(\theta)|$ is near a minimum. That is, at most angles (not too small) $|g|^2 \gg |h|^2$ and $\sigma \approx |g|^2$. However, at or near cross-section minima $|g|^2$ and $|h|^2$ can be of the same order. Since, also, the influence of the MS term is usually stronger on $h(\theta)$ than on $g(\theta)$, the MS effect on polarization can be expected to be non-negligible when $|h| \gtrsim |g|$. At even larger angles, the $\cot\frac{1}{2}\theta$ contribution to $h(\theta)$ becomes very small and even though $d\sigma/d\Omega$ is generally small at these large angles, $g(\theta)$ and $h(\theta)$ are changed so little by the MS term that little effect on the polarization is noted [for example, Bi at 7 MeV and 60° (Fig. 9)].

Since the strength of the nuclear spin-orbit term is not well known, it was varied to study the influence it might have on the calculated polarization curves. At low energies, moderate variations of V_s were found to exert virtually no influence on the polarization curves. For example, for Nb at 0.5 MeV, the curves calculated for $V_s = 7.2$ MeV and $V_s = 10$ MeV were indistinguishable. This confirms similar findings noted in Ref. 7. In order to evaluate this effect at higher energies, Bi polarizations at 7 MeV and 24 MeV were examined for V_s values of 5 MeV and 10 MeV. In general, the polarizations were larger for larger V_s magnitudes as expected, but the changes in polarizations due to the MS term were not substantially effected.

Figures 14 and 15 show small-angle polarizations for Bi at 7 and 24 MeV. The finer angular spacing taken for these calculations shows the polarizations reach nearly 100% at some angle (less than 1°) in both cases. This means, of course, that the wider angular spacing used in the other calculations may not show sufficient detail to give the maximum polarization in all cases. Figure 16 shows the small-angle differential-scattering cross section for Bi at 24 MeV.

These large polarizations (Figs. 14 and 15) could be a useful source of polarized neutrons if one could achieve sufficient collimation to separate the unscattered neutrons from the highly polarized beam scattered at the very small angles.

It is perhaps interesting to note that both the scattering cross section and the polarization are increased at small angles by the MS interaction, whereas one usually finds small cross sections at angles where the polarizations are large.

IV. SUMMARY AND CONCLUSIONS

We conclude with a brief summary and a few statements relative to the conclusions which can be inferred.

Optical-model calculations have been performed to determine the effect of MS scattering on the differential cross section and on the polarization resulting when neutrons are scattered by nuclei. The results are

(1) The differential cross section is influenced only at angles of $\approx 2°$ or less.

(2) The polarization can be influenced at angles much greater than had been previously considered, primarily at angles which lie near minima in the cross-section curve, and at the higher energies considered.

(3) For the energies and nuclei considered, the MS influence tends to be large for large Z and small E,

although the "large-angle" effect is not present for $E<1$ MeV.

(4) Use of the Born approximation to compute that part of the phase shift due to the MS potential is found to be entirely adequate for all cases considered.

One concludes from this that, since the polarization influence of MS scattering extends to large angle for Z not too small, any optical model study which attempts to fit polarization data or to make some evaluation of the nuclear spin-orbit term must include the MS potential. Moderate variations of the nuclear spin-orbit strength around the Perey and Buck value of 7.2 MeV do not significantly influence this conclusion.

An analysis of the influence of the MS force on n-p scattering is in progress and will be submitted for publication in the near future.

ACKNOWLEDGMENTS

The authors are indebted to Battelle-Columbus Laboratories for financial support of this work and to Dr. R. F. Redmond of Battelle, who pointed out the usefulness of Calogero's work and suggested how it might be applied to the present problem. In addition, the assistance of D. L. Beck of Battelle in programming and performing the necessary calculations is gratefully acknowledged.

PHYSICAL REVIEW VOLUME 177, NUMBER 4 20 JANUARY 1969

Projected Hartree-Fock Spectrum of ^{28}Si Including Effects of Pairing and Shape Mixing*

S. N. TEWARI† AND D. GRILLOT‡

Institute of Theoretical Science, University of Oregon, Eugene, Oregon

(Received 9 September 1968)

The energy spectrum of ^{28}Si has been calculated using the angular-momentum states projected from the oblate and the prolate Hartree-Fock solutions. The Hartree-Fock solutions chosen by us take into account all 28 nucleons, and therefore the effect of the polarization of the ^{16}O core has been incorporated into our calculations to some extent. The complexity of the projection calculation has been greatly simplified by suitably using the known symmetries of the Hartree–Fock solutions. The theoretically predicted energy spectrum is compressed by about a factor of 2 when compared with experiment. The small energy gap between the oblate and the prolate Hartree-Fock solutions suggested the possibility of admixing the two solutions by the two-body interaction. The two solutions differ in the four-particle–four-hole states in the intrinsic frame, and therefore the admixture was calculated in the projected basis. The mixing, however, turns out to be too small to affect the spectrum. Another attempt to improve our results was made by including the corrections due to the $T=1$ pairing in the Hartree–Fock solutions, and then calculating the energy spectrum using the states projected from the corrected intrinsic states. The corrections due to the $T=1$ pairing turn out to be of the order of 2% for both the oblate and the prolate Hartree-Fock solutions. This result is consistent with the earlier Hartree-Fock-Bogolyubov calculations on ^{28}Si, which predict no pairing affects. Because of the small size of the pairing corrections, the projected energy spectrum from the corrected intrinsic states does not show any significant improvement.

I. INTRODUCTION

In recent years extensive Hartree–Fock (HF) calculations have been performed for even-even ($N=Z$) nuclei in the 2s, 1d shell.[1–3] For the nuclei in the lower half of the 2s, 1d shell such as ^{20}Ne and ^{24}Mg, with more or less well-defined rotational properties, the results of HF calculations are in reasonably good agreement with the experimental data. It is now believed that the HF theory together with angular-momentum projection techniques provides an extremely satisfactory scheme for carrying out realistic calculations for energy spectra of nuclei having permanent deformations, i.e., rotational properties. For nuclei in the upper half of the 2s, 1d shell such as ^{28}Si and ^{32}S, where there is no conspicuous display of rotational features, the philosophy underlying the HF calculations is to emphasize the qualitative understanding of nuclear properties such as shapes and the nature of deformations. Among these nuclei, ^{28}Si presents a very interesting case.

A number of calculations have been performed for ^{28}Si to determine its intrinsic shape and other properties using phenomenological as well as realistic two-body forces.[2–4] These calculations predict that ^{28}Si has two

* Research sponsored by the Air Force Office of Scientific Research, Office of Aerospace Research, United States Air Force, under Grant No. AF-AFOSR 947-65.

† Present address: Lawrence Radiation Laboratory, University of California, Berkeley, Calif.

‡ Present address: Physics Department, Oregon State University, Corvallis, Ore.

[1] I. Kelson and C. A. Levinson, Phys. Rev. **134**, 269 (1964).

[2] J. Bar-Touv and I. Kelson, Phys. Rev. **138**, 1035 (1965).

[3] M. K. Pal and A. P. Stamp, Phys. Rev. **158**, 924 (1967); A. P. Stamp, Nucl. Phys. **A105**, 627 (1967).

[4] S. Das Gupta and M. Harvey, Nucl. Phys. **A94**, 602 (1967).